Improving surface-based precipitation phase determination through air mass boundary identification

James Feiccabrino, Angela Lundberg and David Gustafsson

ABSTRACT

Most hydrological models apply one empirical formula based on surface air temperature for precipitation phase determination. This approach is flawed as surface precipitation phase results from energy exchanges between falling precipitation and air in the lower atmosphere. Different lower atmospheric conditions cause different precipitation phase probabilities for near-freezing temperatures. Often directly measured lower atmospheric conditions are not available for remote areas. However, meteorological observations occurring before/after similar air mass boundaries have similar atmospheric conditions that vary from most other observations. Therefore, hydrological models can indirectly account for lower atmospheric conditions. Twenty years of manual observations from eight United States weather stations were used to compare misclassified precipitation proportions when analyzing (a) all precipitation observations together and (b) identified cold air mass boundary observations (CAB) and non-CAB observations separately. The CAB observations were identified by a rapid surface air temperature decrease. A two-surface air temperature threshold method with one threshold all snow (T_S°C) and one all rain (T_R°C) having a linear snow fraction decrease between the thresholds was used. The T_S (0 °C), and T_R (4 °C) values for CAB were 1 °C warmer than for non-CAB (−1 °C, 3 °C). Analyzing CAB and non-CAB separately reduced misclassified precipitation 23%, from 7.0 to 5.4%.

Key words | air mass boundary, modeling, precipitation phase, rain, snow

James Feiccabrino (corresponding author)
Angela Lundberg
Applied Chemistry and Geosciences,
Luleå University of Technology,
SE-971 87 Luleå,
Sweden
E-mail: *jamfei@ltu.se*

David Gustafsson
Land and Water Resources Engineering,
Royal Institute of Technology KTH,
SE-100 44 Stockholm,
Sweden

INTRODUCTION

Discrimination between rain and snow remains one of the most important and difficult tasks for hydrologists and meteorologists (Lackmann *et al.* 2002). Loth *et al.* (1993) exemplifies the impact of precipitation phase modeling on snow parameters, for example snow density, albedo, snowpack layering and the water retention capacity of a snowpack. These parameters are important for flood forecasting, hydropower management, and farming (Olson *et al.* 1995). The phase determination is most complicated for surface air temperatures where the precipitation phase probability changes from mostly snow to mostly rain, referred to here as the precipitation phase transition zone (PTZ). For ease of writing this paper will focus on hydrological models. However, this phase discrimination technique can also be useful in engineering, biology, or ecological models.

The relative benefit of improved precipitation phase determination in hydrological models is climate dependent. It is important in regions where a large fraction of winter precipitation falls at near-freezing surface air temperatures (i.e. northern Japan) while it is less important in cold continental climates that have only a few precipitation events with surface air temperatures around zero during the quick (one to two week) cooling and warming periods at the beginning and end of the snow season (i.e. Canada in Fassnacht & Soulis 2002).

Many of today's hydrological models use input data from automated surface weather stations for precipitation phase determination (Feiccabrino & Lundberg 2008). Most of these models use a single empirical formula for a precipitation phase probability scheme (reviewed in Feiccabrino & Lundberg 2009).

These precipitation phase determination schemes are often based on: (a) one single surface air temperature threshold separating rain from snow ($T_{R/S}$) (e.g. 1 °C Aðalgeirsdóttir et al. 2006); (b) two surface air temperature thresholds, one for all snow (T_S) and one for all rain (T_R); with a linear decrease in snow fraction (S_F) for the surface air temperatures in the PTZ (e.g. ACOE 1956); or (c) a snow probability polynomial for surface air temperatures in the PTZ (e.g. Bartlett et al. 2006; based on Auer 1974), see Figure 1. These examples of surface air temperaturebased empirical formulas for precipitation phase determination altogether ignore the lower atmospheric conditions acting on the precipitation (Lundquist et al. 2008).

Using the same $T_{R/S}$, T_S, or T_R value/s for all precipitation observations in a surface air temperature-based precipitation phase determination scheme ignores the meteorological understanding that surface precipitation phase is not determined by surface conditions. Instead surface precipitation phase is a result of latent heat exchanges between falling precipitation and air in the lowest 3 km of the atmosphere, hereafter called the lower troposphere (Carlson 1980; Browning 1986; Fraedrich et al. 1986; Venne et al. 1997; Bourgouin 2000).

The vertical (air) temperature profile of the lower troposphere is not measured by automated surface weather stations. However, similar changes in the vertical temperature profile are expected with similar types of air mass boundaries. Air mass boundary types can be identified by changes in wind speed, wind direction, and surface air temperature (Bjerknes 1919; Fraedrich et al. 1986; Oliver & Oliver 1945; Sanders 1999) when past, current and future surface observations are compared.

The air temperature in a vertical temperature profile through a single air mass can be assumed to cool steadily with height due to a corresponding steady decrease in air pressure (Figure 2(a)). An air mass boundary adds a thin sharp air temperature change between each air mass in a vertical temperature profile (Figures 2(b)–(c)). The presence (Figure 2(b)) or lack of an air mass boundary (Figure 2(a)) above a location affects latent heat exchanges between precipitation and air. Therefore, an air mass boundary present in the lower troposphere changes precipitation phase probabilities at near-freezing temperatures. Considering the above, different types of air mass boundaries should be expected to have different $T_{R/S}$, T_S, and/or T_R values.

Therefore it is proposed that hydrological models can be improved by using different $T_{R/S}$, T_S, or T_R value/s in their precipitation phase probability schemes for different types of air mass boundaries. This improvement specifically addresses the misclassified precipitation associated with warm and cold air advection (air mass boundaries) noted by Loth et al. (1993).

It is also important to realize that there are three main time resolutions used for precipitation phase determination. The longest works with daily average values from meteorological observations. The middle resolution works with hourly resolution of meteorological data. The shortest currently developing resolution works on near live data. This last option integrates weather radar data into the precipitation phase determination scheme. As weather radar can give the height of the melting layer, it is not necessary to use an empirical formula to determine precipitation phase.
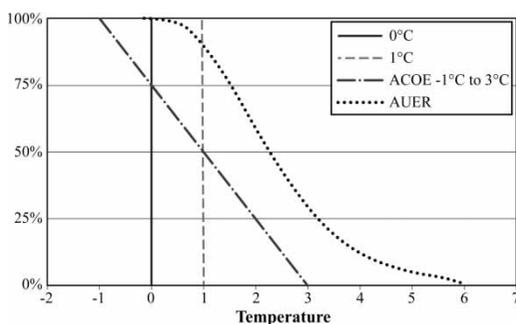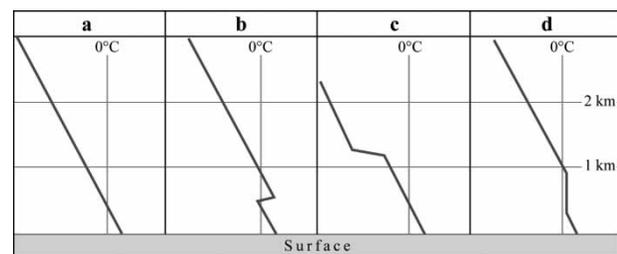

Figure 1 | Examples of snow fraction/temperature relationships commonly used surface in air temperature-based precipitation phase determination schemes.

Figure 2 | Vertical (air) temperature profiles in the lower troposphere for different near-freezing precipitation events: (a) a steadily cooling air temperature with height, without an air mass boundary; (b) an air mass boundary separating a cold (below) and a warm (above) air mass; (c) an air mass boundary separating a warm (below) and a cold (above) air mass; and (d) a steadily cooling air temperature with height interrupted by an isothermal layer created from latent heat released when falling snow melts.

Therefore this method would only work as a back-up for the developing models.

It should also be noted that identification of air mass boundaries in most cases requires surface data with higher temporal resolution than daily averages used in many hydrological models. On the other hand, many models requiring higher time resolution can use this method to determine precipitation phase using automated meteorological data. The method in this paper would also be useful for reanalyzing historical automated weather data.

The objectives here are to show that precipitation phase determination in hydrological models can be improved by air mass boundary identification, and to illustrate the improvement achieved by analyzing easily identifiable air mass boundary observations separately compared to when all precipitation was analyzed together.

To do this, first a basic review of the meteorology associated with air mass boundaries must be given for scientists other than meteorologists, for example hydrologists, engineers, or biologists, to follow. Then, observations affected by similar air mass boundaries must be identified, grouped together, and analyzed for differences in $T_{R/S}$, T_S, or T_R values.

MATERIALS

Manual on the hour winter (November to April) observations from eight weather stations in the United States were provided by the US Air Force Weather Agency. These weather stations represent three different winter regions; the mountain *West*, the flat upper *Plains*, and the hilly *East* influenced by warm Gulf Stream waters (Figure 3

and Table 1). Most of the observations were made between the years 1983 and 2003 but an earlier period was used for station KLIZ which closed in 1991 (Table 1). For each observation the following five minute average conditions were recorded; wind direction to 10° azimuth, wind speed in knots (kts), predominant visibility in meters, up to three precipitation types, and surface air temperature (measured 2 m above ground). Unfortunately, the temperature resolution for these observations was only 1.0 °C, which is often the case for historical weather data in North America.

Review of air mass boundaries

There are several kinds of air mass boundaries and considerable variability among them (Taylor *et al.* 1993). Air mass boundaries keep warm and cold air masses from mixing (Bjerknes & Solberg 1922). The strongest of these boundaries are fronts, which are assumed to behave as solid surfaces extending from the ground to the top of the troposphere (Smith & Reeder 1988).

Frontal boundaries can be recognized at the surface by identifiable characteristics such as a cyclonic (counter-clockwise) wind shift, and a surface air temperature gradient across the boundary (Schultz 2005). Wind speeds are also known to increase at frontal boundaries. Other types of cold/warm air mass boundaries, such as troughs, are usually weaker and lack at least one identifying characteristic of fronts (Sanders 1999; Schultz 2005).

Figure 3 | Location of weather stations.

Table 1 | US Air Force Weather station identification codes with region and time periods used

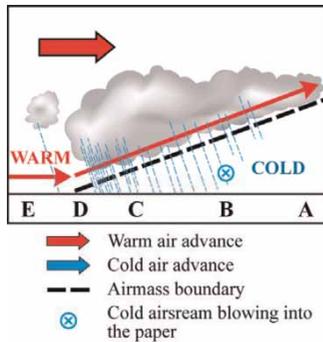| Station	Years	Region	First date	Last date
KMOU	21	West	01 JAN 83	31 DEC 03
KSKA	20	West	01 JAN 83	31 DEC 02
KHIF	17	West	01 JAN 83	31 DEC 99
KMIB	21	Plains	01 JAN 83	31 DEC 03
KRDR	21	Plains	01 JAN 83	31 DEC 03
KRCA	21	Plains	01 JAN 83	31 DEC 03
KNHZ	21	East	01 JAN 83	31 DEC 03
KLIZ	21	East	01 JAN 70	31 DEC 91

Figure 4 | A lower tropospheric cross section perpendicular to a warm frontal boundary where a stationary surface location progresses in time from point A to E.

Figure 5 | A lower tropospheric cross section perpendicular to a cold frontal boundary where a stationary surface location progresses in time from point A to D.

Warm fronts

Warm fronts (WFs) are a subgroup of warm air mass boundaries where cold air is replaced by warm air (Venne *et al.* 1997) (Figures 4(a)–(e)). Precipitation intensity is light and constant, lasting for many hours before surface frontal passage. This is due to the shallow ascent of warm air up the frontal slope (Hanesiak *et al.* 1997), see Figure 4.

Surface identification of some WFs can be difficult due to weak peak winds 8–10 kts (5 m/s), only a 1–2 °C warming of surface air temperature across the boundary, and a slow continuous wind shift (Taylor *et al.* 1993). However, some WFs are well defined with surface air temperature gradients exceeding 10 °C per 100 km (Stewart *et al.* 1995).

The vertical temperature profile during WF precipitation (Figures 4(b)–(d)) has a thin sharp warming of the air temperature between a lower and an upper air mass (Figure 2(b)). This boundary progressively lowers as the surface WF approaches a location.

Cold fronts

Cold fronts are a subgroup of cold air mass boundaries (CAB) where warm air is replaced by cold air (Venne *et al.* 1997) (Figures 5(a)–(d)). There are two types of cold fronts, the one dealt with in this paper is the ana-cold front. Ana-cold fronts (ACFs) have a narrow elongated area (line) of great intensity precipitation before and during frontal passage (Figures 5(b) and (c)). This is caused by the rapid ascension of warm air up a steep frontal slope (Bjerknes 1919; Browning & Monk 1982; Browning 1986; Smith & Reeder 1988; Stewart *et al.* 1995).
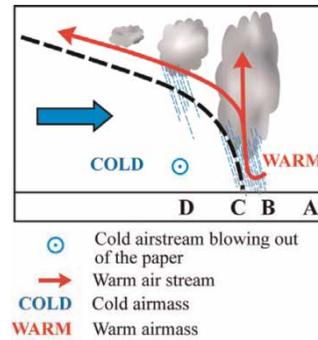
ACFs can be identified at the surface by heavy precipitation, a rapid cyclonic wind shift, high wind velocities (Browning 1986), and a cooling of surface air temperatures across the frontal boundary.

The vertical temperature profile before a surface ACF passage steadily cools with height (Figures 5(b), (c) and 2(a)).

Other common air mass boundaries

The other type of cold front is known as a kata-cold front. Kata-cold fronts have an upper cold frontal boundary (2 to 3 km above the ground) that advances well ahead of its surface cold frontal boundary (Browning 1986). The cold air advancing over warm surface air forms a unique air mass boundary with warm lighter air under dense cold air (Figure 2(c)). On the ground a cyclonic wind shift with a weak surface air temperature cooling can indicate surface or upper kata-cold frontal boundary passage. Little to no precipitation is expected during this surface frontal passage. Kata-cold fronts are therefore difficult to identify at the surface and are not used in this study.

Occlusions are formed when a cold and a WF meet and can have either warming or cooling of surface air temperatures across the surface air mass boundary. When these fronts meet the warm air mass which used to separate cold and WFs is lifted from the surface. The surface air mass boundary for an occlusion then separates the cold air masses associated with pre-WF (Figure 4) and post cold frontal (Figure 5) boundary air (Bjerknes & Solberg 1922). This type of surface air mass boundary is usually weak with little to no change in surface air temperature or wind speed/direction.

A pre-frontal trough usually has a small or negligible surface air temperature decrease across the air mass boundary. It usually occurs ahead of a main cold front having a cyclonic wind shift, but the contrasts in wind or surface air temperature are too weak to be considered a cold front (Schultz 2005).

A baroclinic trough could be a cold or warm air mass boundary. It lacks a cyclonic wind shift, but has many other frontal characteristics (Sanders 1999).

An arctic trough (front) is a baroclinic trough with a sharp boundary of cold polar air moving equatorward (resembling Figure 5). It is characterized by a sharp cooling of surface air temperatures and an increase in wind speed, but little to no cyclonic change in wind direction (Wang *et al*. 1995).

METHODS

The above literature review of air mass boundaries was used to derive a simplified scheme to identify precipitation phase observations affected by similar air mass boundaries. Then observation groups affected by different air mass boundaries were analyzed for changes in their $T_{R/S}$ and their PTZs (i.e. T_S and T_R values). Finally, the percentage of misclassified precipitation observations was compared between (a) all precipitation (AP) observations grouped together for common T_S and T_R values and (b) air mass boundary observation groups analyzed separately for group specific T_S and T_R values.

Air mass boundary passage identification

A simplified guide to surface air mass boundary passage identification was derived from a literature review. The identification scheme is based on wind speed, cyclonic change in wind direction, surface air temperature changes across the air mass boundary (Table 2), and equations similar to those used by Lucas *et al*. (2001).

The guide was applied to each hourly precipitation phase observation to identify the following air mass boundary passage types: WF, CAB, and the CAB subgroup ACF. All observations not belonging to WF, or CAB are classified

Table 2 | Guide to identification of surface air mass boundary passage

Type of front or trough	Acronym	Change in wind direction	Wind speed	Change in temperature
Warm front	**(WF)**	**Strong**	–	**Increase (weak)**
Ana-cold front	**(ACF/ CAB)**	**Strong**	High	**Decrease (strong)**
Kata-cold front (Upper)	–	–	Low	–
Kata-cold front (Lower)	**(CAB)**	**Strong**	Low	**Decrease (weak)**
Occlusion front	–	–	Low	–
Arctic/ barotropic trough	**(CAB)**	Weak	High	**Decrease (strong)**
Pre-frontal trough	**(CAB)**	–	–	**Decrease (–)**

Characteristics of air mass boundary passage in respect to wind speed, changes in wind direction, and changes in surface air temperature. The bold font indicates air mass types and the parameters used to identify them.

as unidentified air mass boundary (UAB) observations. Alternatively, WF and UAB were combined for a group of all non-cold air mass boundary observations (non-CAB). The details of how the different air mass boundary types were identified are given in the following subsections. The parameter values in the equations used to identify air mass boundary observations were selected as a compromise between what could be expected from prior literature, and the necessity to get a reasonable sample size in each group. Two different time windows were used for WF and ACF/CAB, respectively: a 4-hour time step was used for WF due to the shallow frontal surface, while a 2-hour time step was used for both CAB and ACF due to steeper frontal slopes.

Classification of warm frontal zones

A WF zone was identified by the following four-hour conditions (Equation (1)): (a) the surface air temperature during an observation (T_t) was at least 2 °C warmer than an observation four hours before (T_{t-4}), (b) the wind speed at the end of the observation period (wS_t) was greater than or equal to 15 knots (8 m/s), and (c) a cyclonic change in wind direction (wD) between $30°$ and $180°$ had occurred

during the period:

$$\text{If } [(T_t - T_{t-4}) \geq 2\,°C] \text{ and } [wS_t \geq 15\,\text{kts}] \text{ and}$$
$$[30° \leq (wD_t - wD_{t-4}) \leq 180°] \tag{1}$$

then the event was classified as a WF zone with a surface WF passage at the time of the last observation. The identified WF group accounted for 1% of AP (Figure 6).

Classification of cold air mass boundary zones

A CAB zone was identified by the following two-hour condition (Equation (2)): the surface air temperature two hours before an observation (T_{t-2}) was at least $2\,°C$ warmer than during an observation (T_t):

$$\text{If } [(T_{t-2} - T_t) \geq 2\,°C] \tag{2}$$

then the event was classified as a CAB zone, with a surface CAB passage at the time of the last observation. The identified CAB group, always including ACF, accounted for 12% of AP (Figure 6).

Classification of ana-cold frontal zones

An ACF zone is a CAB zone (above) with two additional two-hour conditions (Equation (3)): (a) the wS_t at the end of the observation period was greater than or equal to 15 kts, and (b) a cyclonic change in wD between 30° and 180° had occurred during the period:

$$\text{If } [(T_{t-2} - T_t) \geq 2\,°C] \text{ and } [wS_t \geq 15\,\text{kts}] \text{ and}$$
$$[30° \leq (wD_t - wD_{t-2}) \leq 180°] \tag{3}$$

then the event was classified as an ACF zone, with a surface ACF passage at the time of the last observation.
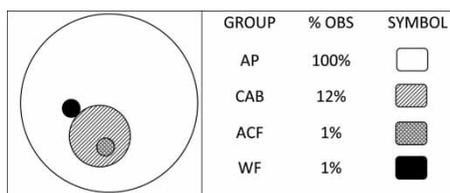

Figure 6 | Frequency of observation groups.

The identified ACF group accounted for 1% of AP (Figure 6).

Precipitation phase observations between -1 and $5\,°C$ were first categorized as; *snow* for snow, graupel, and ice pellets, *freezing* for freezing rain, and freezing drizzle, *rain* for rain, and drizzle, and *mixed* for any combination of the above categories. Following the example of previous precipitation phase probability studies, freezing phase observations were excluded from the analysis. To omit low intensity precipitation, observations were only included when visibilities were 9,000 m or less, as hourly manual observations do not include precipitation totals. However, if a data set was available with precipitation totals 0.01 in or 0.1 cm would have been appropriate hourly precipitation totals.

Single-threshold method

As the observations were made in whole degrees Celsius shifts in $T_{R/S}$ smaller than one degree would not be possible to detect so the analysis was made in two steps. First the $T_{R/S}$ values were determined. Then the amount of misclassified precipitation using these $T_{R/S}$ values was determined.

For each group of observations classified by air mass boundary passage type a $T_{R/S}$ was set to the warmest surface air temperature on a $1.0\,°C$ scale with at least 50% of the observations classified as snow. Observations with surface air temperatures (T) at and colder than the $T_{R/S}$ were treated as 100% snow, while observations with surface air temperatures warmer then the $T_{R/S}$ were treated as 100% rain. Any snow observations with surface air temperatures warmer, or rain observations with surface air temperatures at or colder than a $T_{R/S}$ were considered misclassified precipitation (Equation (4)) (Figures 7 and 8):

$$S_F = 1 \quad \text{for } T \leq T_{R/S}; \quad S_F = 0 \quad \text{for } T > T_{R/S} \tag{4}$$

Two-threshold method

Surface air temperatures with a misclassified precipitation rate over 10% in the $T_{R/S}$ scheme above were regarded as part of a PTZ where $1 > S_F > 0$. The T_S and T_R values were set one surface air temperature step wider than the PTZ.
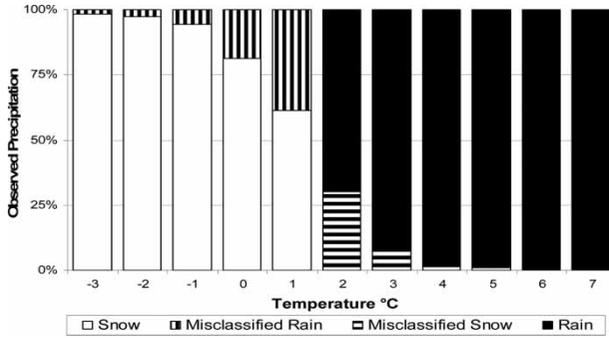
Figure 7 │ Observed percentages of rain and snow with misclassified rain and snow using a single surface air temperature threshold scheme at 1 °C.
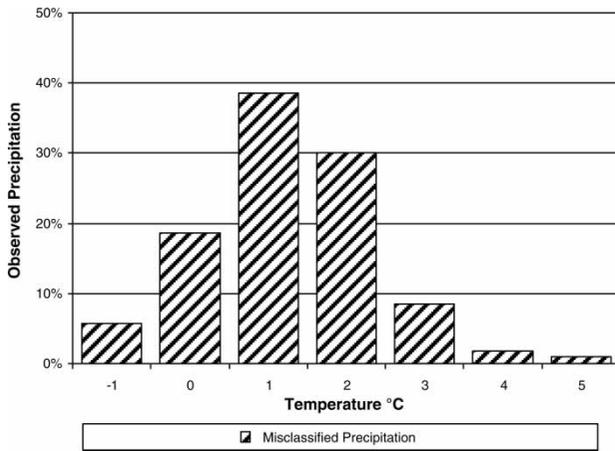

Figure 8 │ Misclassified precipitation (rain and snow) percentages from Figure 7.

The S_F was then assumed to decrease linearly from T_S to T_R (Equation (5)):

$$S_F = 1 \quad \text{for } T \leq T_s; \quad S_F = 0 \quad \text{for } T \geq T_R;$$
$$S_F = 1 - \frac{T - T_S}{T_R - T_S} \quad \text{for } T_S \leq T \leq T_R. \tag{5}$$

For each air mass boundary group a two surface air temperature threshold scheme with optimized T_S and T_R values were then used to calculate the snow fractions ($S_F^{Calculated}$) for each 1.0 °C temperature step. The difference between $S_F^{Calculated}$ and observed snow fraction (S_F^{Obs}) gives the misclassified precipitation (ε) for a single surface air temperature using a precipitation phase determination scheme:

$$\varepsilon = S_F^{Calculated} - S_F^{Obs}. \tag{6}$$

A positive ε represents the fraction of rain misclassified as snow for a surface air temperature. Therefore, a negative ε represents the fraction of snow misclassified as rain.

Treatment of mixed precipitation

Of note, mixed precipitation observations are generally ignored when determining precipitation phase determination schemes (Bartlett *et al.* 2006). However, the treatment of mixed precipitation should be considered for precipitation phase probability schemes focusing on the PTZ. A large fraction of precipitation was found to be mixed for surface air temperatures between −1 and 5 °C, especially for the group of CAB observations (Figure 9). The analysis above was made excluding mixed precipitation, but a check was then made to see if the result would have been different if the mixed precipitation was included.

The treatment of mixed precipitation could affect the $T_{R/S}$, T_S, or T_R values determined with Equations (1) and (2). Therefore, these threshold values were calculated to check for changes when mixed precipitation was analyzed as all rain, all snow (Bartlett *et al.* 2006), or ignored (Fassnacht & Soulis 2002).

Misclassified precipitation comparison

For each of the classified groups (CAB, Non-CAB and AP) misclassified precipitation was determined using both a one and a two-threshold scheme. The analysis was made for the surface air temperature range −1 to 5 °C and
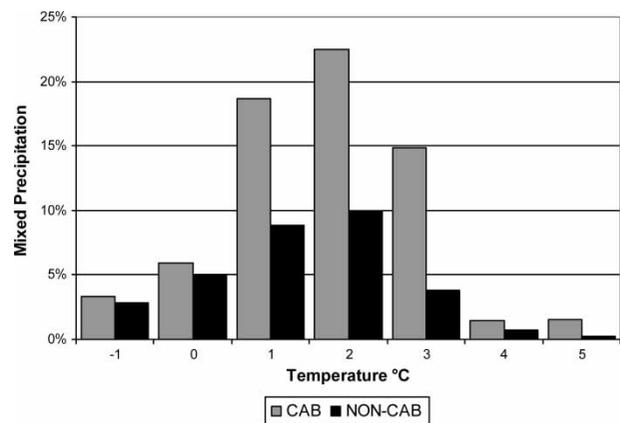

Figure 9 │ Observed percentage of mixed precipitation for the identified cold air mass boundaries (CAB) and for the non-CAB.

followed the approach by Kongoli & Bland (2000):

Misclassified Precipitation

$$= \frac{\sum \text{misclassified snow} + \sum \text{misclassified rain}}{\sum \text{observed precipitation}} \quad (7)$$

RESULTS

The results below are organized in the following steps; first an air mass boundary precipitation phase probability was made without mixed precipitation, then the effect of including mixed precipitation into this analysis is presented and finally the total improvement in precipitation phase determination when identified air mass boundary observations were analyzed separately.

Precipitation phase probability analysis with and without mixed precipitation

The $T_{R/S}$ values determined from the S_F^{Obs}, without mixed precipitation, were found to be $1\,^{\circ}C$ for AP and WF and $2\,^{\circ}C$ for ACF (Figure 10).

Treating the mixed precipitation as all rain, or all snow did not alter these found $T_{R/S}$ values. However, when mixed precipitation was treated as all snow the $T_{R/S}$ for CAB changes from $1\,^{\circ}C$ (without mixed precipitation) to $2\,^{\circ}C$ (Figure 11). Treatment of mixed precipitation had no affect on the T_R or T_S values for any of the observation groups. As mixed precipitation observations only affects the $T_{R/S}$ for CAB, and the snow to rain ratio for mixed precipitation is
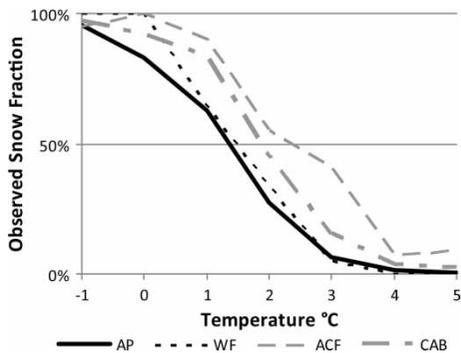

Figure 11 | Observed snow fraction for all observations in the CAB group with mixed precipitation treated as all snow, as all rain, or ignored.

unknown, further analysis is performed without mixed precipitation observations.

Misclassified precipitation comparison

The distribution of misclassified precipitation for UAB and WF were similar (Figure 12). Both groups have a maximum misclassified precipitation at $1\,^{\circ}C$, their optimized $T_{R/S}$ value, and a PTZ with $T_S = -1\,^{\circ}C$ and $T_R = 3\,^{\circ}C$ values. Due to the above similarities, WF and UAB were combined to form a group of non-CAB observations.

The maximum misclassified precipitation for both CAB and ACF occurred at $2\,^{\circ}C$ (Figure 13), $1\,^{\circ}C$ warmer than the maximum for non-CAB (Figure 12). The PTZ for both CAB and ACF ($T_S = 0\,^{\circ}C$ and $T_R = 4\,^{\circ}C$) shift $1\,^{\circ}C$ warmer than the PTZ for non-CAB (Figure 13). All PTZs were found to have a $4\,^{\circ}C$ temperature range (Figures 12 and 13).

Figure 10 | Observed snow fraction for all grouped observations; all precipitation (AP), ana-cold frontal zone (ACF), warm frontal zone (WF), and cold air mass boundary zone (CAB) without mixed precipitation.
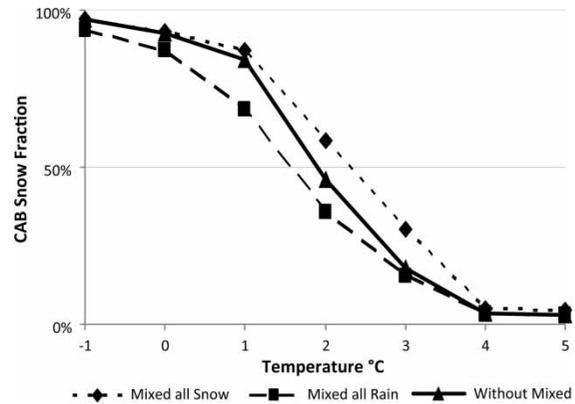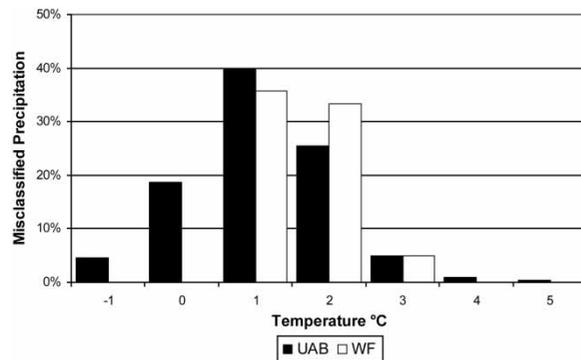

Figure 12 | Percentage of misclassified precipitation observations using $T_{R/S} = 1\,^{\circ}C$ for warm frontal zone (WF) and unidentified air mass boundary (UAB).
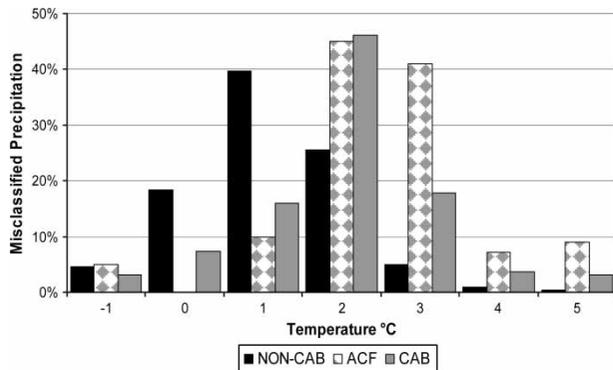
Figure 13 │ Percentage of misclassified precipitation observations using $T_{R/S} = 1\,°C$ for cold air mass boundaries (CAB) and non-CAB observations, and $T_{R/S} = 2\,°C$ for ana-cold fronts (ACF).

DISCUSSION

The results show that air mass boundary identification will improve precipitation phase determination for hydrological models using input data from automated weather observations. A discussion of method assumptions and weaknesses, applications and future work follows.

This method links changes in the PTZ surface air temperatures to a relative time before (or after) a surface air mass boundary passes a location. However, the length of time a WF or CAB affects the lower troposphere over a location varies with air mass boundary speed, angle of warm air ascent, and to what extent the air mass boundary is moving parallel or perpendicular to the location. For this reason, a 4-hour time step was used for the slower shallower sloping WF zones (Figure 4) and a 2-hour time step was used for the faster and steeper sloping CAB zones (Figure 5). The WF and CAB zones were chosen for their obvious difference in expected vertical (air) temperature profiles.

A contrast between observation groups is required for this method to be useful, therefore the time steps used are important. If the time steps are too large observations not affected by air mass boundary changes in the near-surface vertical temperature profile will also be included in the group of observations affected by an air mass boundary. This will weaken the contrast between the air mass boundary observation group and all other observations. However, if the time steps are too small air mass boundary observation groups (e.g. ACF) could have a strong contrast

At a 1 °C scale there was no change in the $T_{R/S}$ between CAB, and non-CAB. Therefore no change occurred when using a $T_{R/S}$ scheme at this surface air temperature scale. However, as the PTZs for the groups were found to be different, applying a universal and group specific T_S and T_R scheme produced different results.

Determined from AP the universal values in a T_S (−1 °C), T_R (3 °C) scheme produced 7% misclassified precipitation for AP, 16% for CAB and 5% for non-CAB (Table 3). However using the CAB-specific T_S (0 °C), T_R (4 °C) values reduced misclassified precipitation within CAB from 16% to 6%. This reduced the total amount of misclassified precipitation from 7 to 5.4%, corresponding to a total reduction of 23% in misclassified precipitation.

Table 3 │ Total number of observations (# Obs) with the percent misclassified precipitation (error) using universal values, T_S (−1 °C) and T_R (3 °C), in a two surface air temperature threshold scheme (Equation (1)), on all precipitation observations, cold air mass boundary observations (CAB), and all non-CAB observations

Temperature (°C)	All precipitation		Cold air mass boundary				Non-cold air mass boundary	
	Error (%)	# Obs	Error (%)	CAB error (%)	# Obs	% of total obs (%)	Error (%)	# Obs
−1	−4	4.263	−3	−3	639	15	−5	3.630
0	8	3.474	18	−7	479	14	7	2.998
1	13	5.346	34	9	540	10	10	4.811
2	3	3.187	21	−4	297	9	1	2.893
3	6	2.213	18	−7	235	11	5	1.979
4	1	1.865	4	4	273	15	1	1.594
5	1	838	3	3	127	15	0	712
Total error	7		16	6			5	

Error using T_S (0 °C) and T_R (4 °C) values were calculated for CAB observations (CAB error). CAB error was calculated similarly using a T_S (0 °C) and T_R (4 °C).

compared to all other observations, but the number of separated observations may be too few to have a meaningful effect on overall precipitation phase determination.

All observations in each group are here assumed to have approximately the same lower tropospheric conditions acting on precipitation. However, in reality each individual air mass boundary observation has its own unique vertical temperature profile. Variability is added to vertical temperature profiles (Figures 2(a)–(c)) when melting (Figure 2(d)) and freezing precipitation are accounted for (see Kain *et al.* 2000). Frozen precipitation will melt when falling through an isothermal layer slightly warmer than freezing. This melting absorbs latent heat from the environment, thus cooling the layer (Bourgouin 2000; Lackmann *et al.* 2002). The opposite will occur if liquid precipitation freezes in a sub-freezing atmospheric layer.

The vertical temperature profile above a location was in this study assumed to have either zero or one air mass boundaries. However, there is sometimes more than one air mass boundary above a location or multiple freezing levels (see Hux *et al.* 2001). It was also assumed that temperature decreases steadily with height in an air mass. However, vertical temperature decrease is somewhat variable, especially when air changes from dry (clear) to moist (clouds).

This method also relies on air mass boundaries being identified at the surface. However, surface air mass boundaries can discontinuously advance across large regions and therefore not always be identified at the surface (Smith & Reeder 1988; Bryan & Fritsch 2000). Even when air mass boundaries exist at the surface they may not be identifiable (Fraedrich *et al.* 1986). Relations used to identify air mass boundaries differ between authors, for example Fraedrich *et al.* (1986) used only a surface air temperature change greater than or equal to 3 °C per 100 km to identify fronts, while many authors including Anderson (1990) and Taylor *et al.* (1993) consider a cyclonic wind shift to be the best indicator of frontal boundaries. In this paper both of these methods were used, the first to identify general CAB, while the latter was used to identify ACF and WF.

The requirements for air mass boundary identification were here kept simple allowing multiple types of air mass boundaries to be lumped into only a few categories. According to Table 2, Equation (1) should identify strong WF zones and possibly some occlusions. Equation (2) should identify

ACF, some strong occlusions, arctic troughs and possibly some pre-frontal troughs. Equation (3) should identify ACF and rare cases of strong occlusions or pre-frontal troughs. The remaining observations should then consist of most occlusions, pre-frontal troughs, some baroclinic troughs, weak WF, upper and lower kata-cold fronts, WF precipitation occurring more than four hours before frontal passage, orographic precipitation, and the rare winter convective storm.

The analysis here excluded observations with visibilities greater than 9,000 m and freezing precipitation. Precipitation observations with visibilities greater than 9,000 m contribute little to precipitation totals, so they must be kept from having too large an effect on the analysis. Observations with freezing precipitation were excluded as their inclusion as snow or rain is model dependent, and they have little impact on the studied temperature range.

Mixed precipitation observations were considered but ultimately excluded from the analysis. Mixed precipitation is usually excluded as phases other than rain or snow are generally not recognized in surface schemes (Bartlett *et al.* 2006). Few studies focus on the ratio of snow to rain in mixed precipitation and the studies that are available (Stewart *et al.* 1984; Yuter *et al.* 2006) are short term, usually analyzing a single storm. In-flight measurements of air temperature and precipitation images suggested that between 0 °C and 0.5 °C in-cloud precipitation was mostly snow, but by 1.3 °C almost all was rain (Stewart *et al.* 1984). Another study using the surface weather observations of temperature and precipitation type at different elevations on a mountain and the elevation of a radar bright band found the rain fraction to be 1% in the isothermal layer zero degrees, 4% from 0 to 0.5 °C, and 93% between 0.5 and 1.5 °C (Yuter *et al.* 2006). This means that the mixed precipitation should change from mostly snow to mostly rain over a less than 1 °C surface air temperature range (Stewart *et al.* 1984; Yuter *et al.* 2006).

There is no standard approach for including mixed precipitation in surface-based precipitation phase probability analysis (Bartlett *et al.* 2006). In prior studies, observed mixed precipitation has been treated either (1) as all snow (Bartlett *et al.* 2006); (2) as all rain; or (3) excluded (Fassnacht & Soulis 2002) (Figure 11). The actual S_F of the mixed precipitation is expected to be somewhere between the first two approaches. The third approach, neglecting

mixed precipitation, meets this expectation. With this approach, below the $T_{R/S}$ value the S_F resembles approach (1), above the $T_{R/S}$ value the S_F resembles approach (2) and at the $T_{R/S}$ itself the S_F is about halfway between the two first approaches (see Figure 11). With approach (3), used here, the mixed precipitation below the $T_{R/S}$ value is considered mostly rain, and above the $T_{R/S}$ the mixed precipitation is considered mostly snow. This agrees well with the findings of Stewart *et al.* (1984) and Yuter *et al.* (2006). Therefore in this data set it is justified to ignore mixed precipitation in the precipitation phase probability analysis.

Improved precipitation phase determination with air mass boundary identification was found to be useful in a two-temperature threshold scheme. This improvement will be important in areas with much, and minor in areas with little, precipitation in the PTZ.

Many hydrological models assume mixed precipitation based on the probability of either rain or snow in a much wider temperature range than used here. Bartlett *et al.* (2006) showed that mixed precipitation occurs much less often than long term trends suggest, but a model using the Auer polynomial handled precipitation in the PTZ better than a model using $T_{R/S} = 0\ °C$.

Improved precipitation phase determination should allow for improved modeling of many precipitation phase-based output values, for example sublimation in tree canopies (Lundberg *et al.* 2004), and glacial mass balance (Aðalgeirsdóttir *et al.* 2006). These improvements can also have economic value in water management for recreation, hydropower production, city planning, and farming (Olson *et al.* 1995). Changing the precipitation phase determination scheme in climate models will affect snow covered area and snowmass estimates. This changes the modeled feedback mechanisms leading to altered local and global climate change estimates (Loth *et al.* 1993). A correct determination of the precipitation phase is important not only for the mass balance of simulated snow covers, but also for the energy balance of the land surface, due to the large negative latent heat content in snow compared to rain. Snow fall could be regarded as a negative heat flux to the land surface, whereas rainfall could be a positive heat flux. Accurate classification of rain and snow is also important for the albedo of the land surface, which indirectly alters the land surface energy balance.

Though not perfect, the method here is a substantial improvement on the current precipitation phase determination methods used in many hydrological models. The method can be implemented into current models without much difficulty as it only uses surface weather observations already applied in hydrological modeling. The main limitation compared to previous methods used for hydrological modeling might be the use of hourly data, as well as the need to include the additional variables needed for the identification of air mass boundaries.

This analysis was based on 2–4-hour time steps. A more thorough analysis is required in order to determine the optimum time steps and whether the 24-hour time step, used by many modelers, can be used. The most obvious problems to be solved with a 24-hour time step would be caused by changes in cloud cover. On a cloudy night the average temperature would appear to be much warmer than a clear night, likewise a clear day may appear much warmer than a cloudy day even after a CAB.

Future work should be done to expand this method by separating more of the easily identified areas of mid-latitude cyclones for analysis such as; post CAB and WF precipitation. A more detailed statistical study could be completed as the misclassified precipitation (Figure 8) has a normal distribution. Given a finer air temperature resolution data set the maximum misclassified precipitation would be approximately 50% at the $T_{R/S}$, which corresponds with the mean (μ), having rain (warmer) error and snow (colder) error decreasing on either side of μ. A 2^k factorial experimental design (Montgomery 2009) could be used to check if other factors such as dew point or wind speed should be included.

Some national weather services have historical weather records with surface air temperatures at a 0.1 °C scale and it would be interesting to employ a similar study using temperatures with a 0.1 °C scale to confirm and expand the findings of this study. A study linking changes in the PTZ with vertical temperature profile measurements would also be useful in supporting the background and reasoning for this method.

CONCLUSIONS

This paper outlines a promising method to reduce the amount of misclassified precipitation in hydrological

models by separating observations into air mass boundary categories. This separation can be done using easily identifiable surface air mass boundary characteristics such as surface air temperature, wind speed and wind direction.

CAB observations were identified by a surface air temperature decrease of 2 °C over a 2 hour period and were found to constitute 12% of all precipitation.

Analyzing CAB separately from all other non-CAB observations reduced the total proportion of the misclassified precipitation observations from 7 to 5.4% (total reduction of error = 23%) when a two surface air temperature threshold scheme was applied. This improvement would have been even greater if precipitation intensity was used rather than number of observations, as CAB usually has higher precipitation intensities than other observations. The improvement by separating CAB was expected due to the differences between vertical air temperature profiles for CAB and most other precipitation observations. Therefore similar results should be found anywhere this approach is applied.

Little improvement in misclassified precipitation was expected or found when WF zone observations were analyzed separate from all other observations. This is because most winter precipitation is the result of frontal lift caused by air mass boundaries. With the exception of kata-cold fronts (Figure 2(c)), air mass boundaries generally separate a cold (below) and a warm (above) air mass. Excluding pre-CAB precipitation (Figure 2(a)), the remaining precipitation occurs with a similar air mass boundary affect on the vertical air temperature profile (Figure 2(b)). However, changes in the S_F for different non-CAB groups may still be possible to identify if a finer temperature scale is used.

Applying a $T_{R/S}$, as is used in many hydrological models, was useful to obtain normal distributions for misclassified precipitation. This will be useful for later statistical studies. However, at a 1 °C scale the difference in $T_{R/S}$ values between observation groups was too small.

ACKNOWLEDGEMENTS

REFERENCES

ACOE, US Army Corps of Engineers 1956 *Snow Hydrology: Summary Report of the Snow Investigations*. North Pacific Division, Portland, OR.

Aðalgeirsdóttir, G., Jóhannesson, T., Björnsson, H., Pálsson, F. & Sigurðsson, O. 2006 Response of Hofsjokull and southern Vanajokull, Iceland, to climate change. *J. Geophys. Res.* **111**, 1–15.

Anderson, C. 1990 Estimating the propagation velocity of atmospheric fronts from surface wind observations. *Atmos. Ocean.* **28** (3), 330–344.

Auer Jr., A. H. 1974 The rain versus snow threshold temperatures. *Weatherwise*. **27**, 67.

Bartlett, P. A., MacKay, M. D. & Verseghy, D. L. 2006 Modified snow algorithms in the Canadian land surface scheme: model runs and sensitivity analysis at three boreal forest stands. *Atmos. Ocean.* **44** (3), 207–222.

Bjerknes, J. 1919 On the structure of moving cyclones. *Geof. Publ.* **1** (2), 1–8.

Bjerknes, J. & Solberg, H. 1922 Life cycle of cyclones and the polar front theory of atmospheric circulation. *Geof. Publ.* **3** (1), 3–18.

Bourgouin, P. 2000 A method to determine precipitation types. *Weather Forecasting* **15**, 583–592.

Browning, K. 1986 Conceptual models of precipitation systems. *Weather Forecasting* **1**, 23–41.

Browning, K. & Monk, G. 1982 A simple model for the synoptic analysis of cold fronts. *Quart. J. R. Met. Soc.* **108**, 435–452.

Bryan, G. & Fritsch, M. 2000 Diabatically driven discrete propagation of surface fronts: a numerical analysis. *J. Atmosph. Sci.* **57**, 2061–2079.

Carlson, T. 1980 Airflow through midlatitude cyclones and the comma cloud pattern. *Monthly Weather Rev.* **108**, 1498–1509.

Fassnacht, S. R. & Soulis, E. D. 2002 Implications during transitional periods of improvements to the snow processes in the land surface scheme–hydrological model WATCLASS. *Atmos. Ocean.* **40** (4), 389–403.

Feiccabrino, J. & Lundberg, A. 2008 Precipitation phase discrimination by dew point and air temperature. In *Proc. 75th Western Snow Conf.*, Kailua-Kona, HI, pp. 141–146.

Feiccabrino, J. & Lundberg, A. 2009 Optimizing precipitation phase discrimination through a climatological study. In *Proc. 65th Eastern snow conf.*, Fairlee, VT, May 2008.

Fraedrich, K., Bach, R. & Naujokat, G. 1986 Single station climatology of central European fronts: number, time and precipitation statistics. *Beitr. Phys. Atmoshp.* **59** (1), 54–65.

Hanesiak, J., Stewart, R., Szeto, K., Hudak, D. & Leighton, H. 1997 The structure, water budget, and radiational features of a high-latitude warm front. *J. Atmosph. Sci.* **54** (12), 1553–1573.

Hux, J. D., Knappenberger, P. C., Michaels, P. J. & Stenger, P. J. 2001 Development of a discriminate analysis mixed precipitation (DAMP) forecast model for mid-atlantic winter storms. *Weather Forecasting* **16**, 248–259.

Kain, J., Goss, S. & Baldwin, M. 2000 The melting effect as a factor in precipitation-type forecasting. *Weather Forecasting* **15**, 700–714.

Kongoli, C. E. & Bland, W. L. 2000 Long-term snow depth simulations using a modified atmosphere-land exchange model. *Agric. For. Meteorol.* **104** (4), 273–287.

Lackmann, G., Keeter, K., Lee, L. & Ek, M. 2002 Model representation of freezing and melting precipitation: implications for winter weather forecasting. *Weather Forecasting* **17**, 1016–1033.

Loth, B., Graf, H. F. & Oberhuber, J. M. 1993 Snow cover model for global climate simulations. *J. Geophys. Res.* **98** (D6), 10451–10464.

Lucas, C., May, P. & Vincent, R. 2001 An algorithm for the detection of fronts in wind profiler data. *Weather Forecasting* **16**, 234–247.

Lundberg, A., Nakai, Y., Thunehed, H. & Halldin, S. 2004 Snow accumulation in forests from ground and remote-sensing data. *Hydrol. Proc.* **18**, 1941–1955.

Lundquist, J. D., Neiman, P. J., Martner, B., White, A. B., Gottas, D. J. & Ralph, F. M. 2008 Rain versus snow in the Sierra Nevada, California: comparing Doppler profiling radar and surface observations of melting level. *J. Hydrometeorol.* **9** (2), 194–211.

Montgomery, D. C. 2009 *Design and Analysis of Experiments.* 7th edition, Wiley, pp. 227–257.

Oliver, V. J. & Oliver, M. B. 1945 Weather analysis from single-station data. In: *Handbook of Meteorology* (F. A. Berry, E. Bolay & N. R. Beers, eds.). McGraw-Hill, New York, pp. 858–879.

Olson, D., Junker, N. & Korty, B. 1995 Evaluation of 33 years of quantitative precipitation forecasting at the NMC. *Weather Forecasting* **10**, 498–511.

Sanders, F. 1999 A proposed method of surface map analysis. *Monthly Weather Rev.* **127**, 945–955.

Schultz, D. 2005 A review of cold fronts with prefrontal troughs and wind shifts. *Monthly Weather Rev.* **133**, 2449–2472.

Smith, R. & Reeder, M. 1988 On the movement and low-level structure of cold fronts. *Monthly Weather Rev.* **116**, 1927–1944.

Stewart, R. E., Bachand, D., Dunkley, R. R., Giles, A. C., Lawson, B., Legal, L., Miller, S. T., Murphy, B. P., Parker, M. N., Paruk, B. J. & Yau, M. K. 1995 Winter storms over Canada. *Atmospheric – Ocean.* **33** (2), 223–247.

Stewart, R. E., Marwitz, J. D., Pace, J. C. & Carbone, R. E. 1984 Characteristics through the melting layer of stratiform clouds. *J. Atmos. Sci.* **41**, 3227–3237.

Taylor, P., Salmon, J. & Stewart, R. 1993 Mesoscale observations of surface fronts and low pressure centers in canadian east coast winter storms. *Boundary-Layer Meteorol.* **64**, 15–54.

Venne, M., Jasperson, W. & Venne, D. 1997 *Difficult Weather: a Review of Thunderstorms, Fog, and Stratus, and Winter Precipitation Forecasting.* Technical Report #A246633. AIRFM Command http://DTIC.mil.

Wang, P., Martin, J., Locatelli, J. & Hobbs, P. 1995 Structure and evolution of the winter cyclones in the central United States and their effects on the distribution of precipitation part II: arctic fronts. *Monthly Weather Rev.* **123**, 1328–1344.

Yuter, S. E., Kingsmill, D., Nance, L. B. & Löffler-Mand, M. 2006 Observations of precipitation size and fallspeed characteristics within coexisting rain and wet snow. *J. Appl. Meteor. Climatol.* **45**, 1450–1464.